Tiny groups of galaxies remember their cosmic origins

~~Detection of the large-scale tidal field with galaxy multiplet alignment in the DESI Y1 spectroscopic survey~~

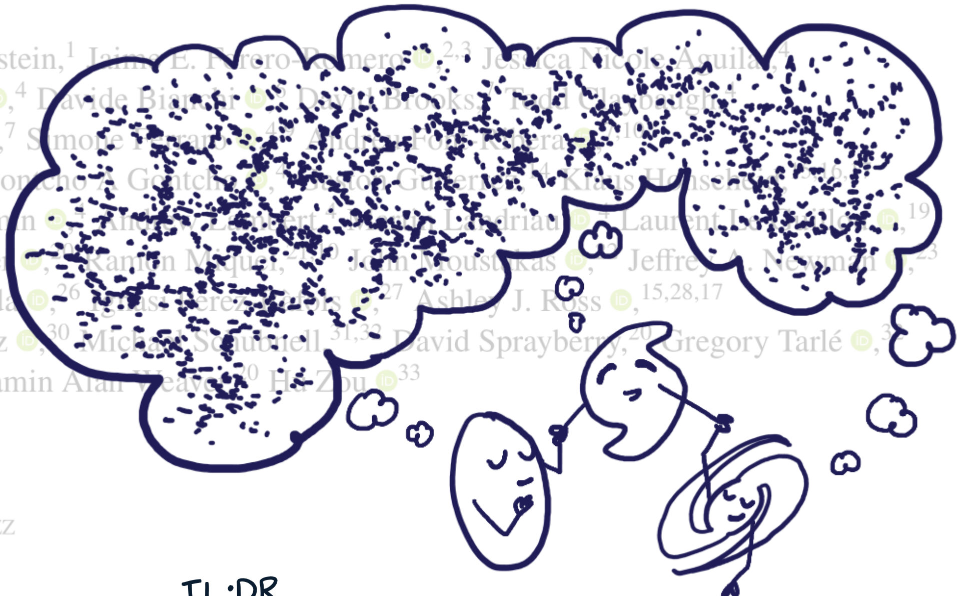

TL;DR

We found a connection between little groups of galaxies, or "multiplets", and the largest structures in the universe. This is cool because usually stuff on small scales seems to forget the cosmic web it originated from. We find that all multiplets remember the same large-scale structure, regardless of the type of galaxies in them. This method doesn't have the main issues that affect similar types of measurements, so it could be a useful way to measure the cosmic web.

The more we know about the cosmic web, the more we know about the stuff that shapes it: like dark energy

BACKGROUND INFO

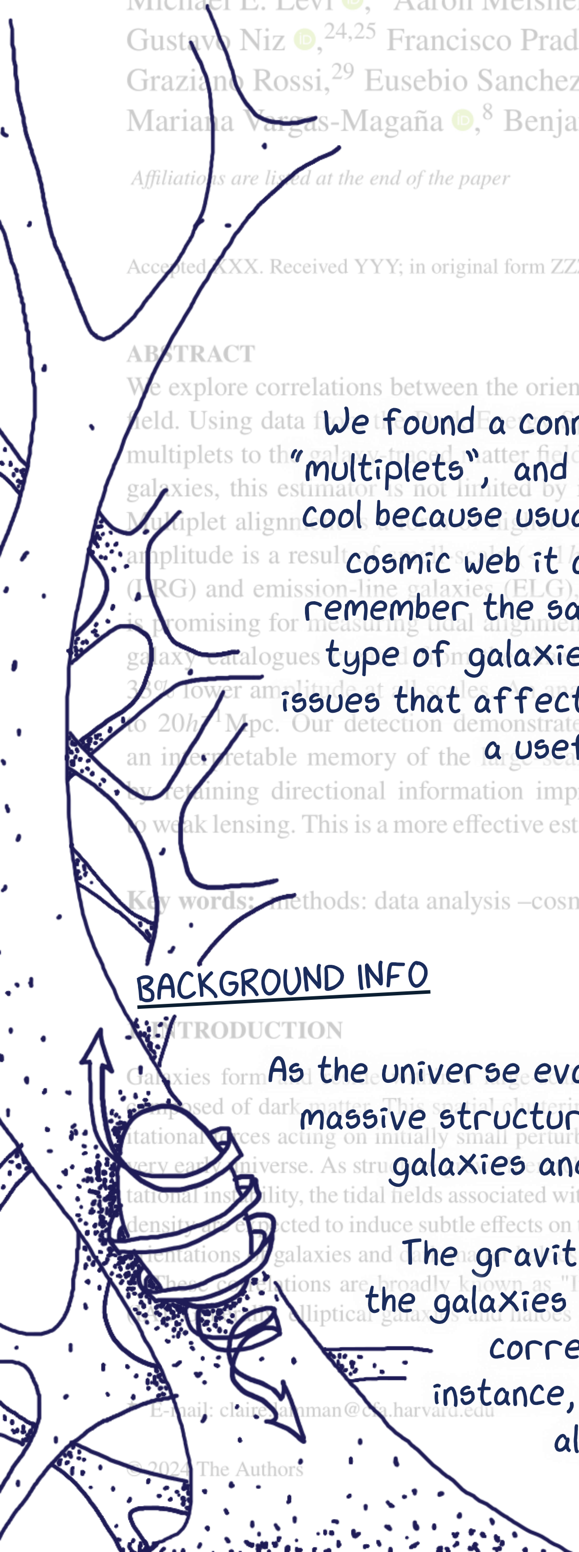

As the universe evolves, gas and dust fall along massive structures of dark matter, forming galaxies and illuminating the cosmic web.

The gravity of the cosmic web affects the galaxies that form along it, creating correlations between the two. For instance, a long galaxy will tend to be aligned along a cosmic strand.

Although we can't see dark matter (it's dark!), we can look at galaxy shapes to figure out more about the invisible structure around it.

However, there are some issues with this approach....

Many people have measured connections between galaxy shapes and the large-scale structure of the universe. The two main difficulties they face are:

1. You need really good pictures of galaxies to precisely measure their shapes (this is hard).

2. Many galaxies show no correlation. No one has been able to make this measurement with spiral galaxies.

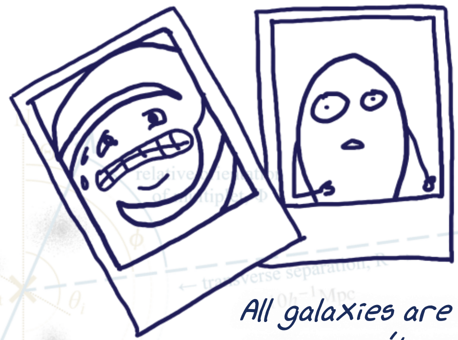

All galaxies are beautiful, but some aren't very photogenic.

...so here's our idea:

Instead of galaxy shapes, let's try using the orientation of tiny groups of galaxies

(We'll explain exactly what this means later)

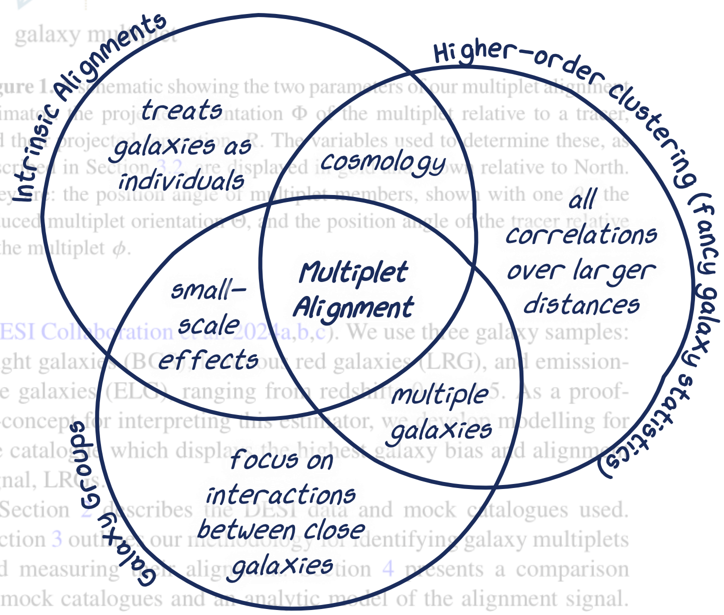

This idea is built upon the work of past scientists and has many connections to it.

WHERE DOES OUR DATA COME FROM?

Only the most AMAZING TELESCOPE EVER!!!! (although I may be a bit biased)

DESI, or the "Dark Energy Spectroscopic Instrument", sits atop a mountain in Arizona. Inside it are 5000 individually-controlled robots. These allow us to measure the distances to thousands of galaxies in mere minutes.

DESI is in the middle of its 5-year survey, but has already created the most detailed map of the nearby universe!

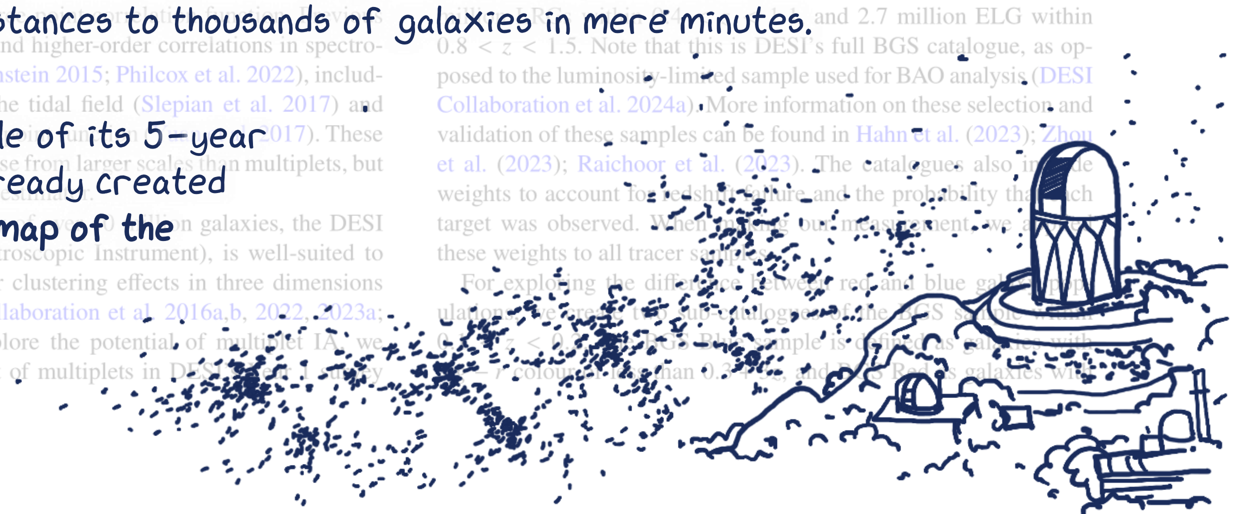

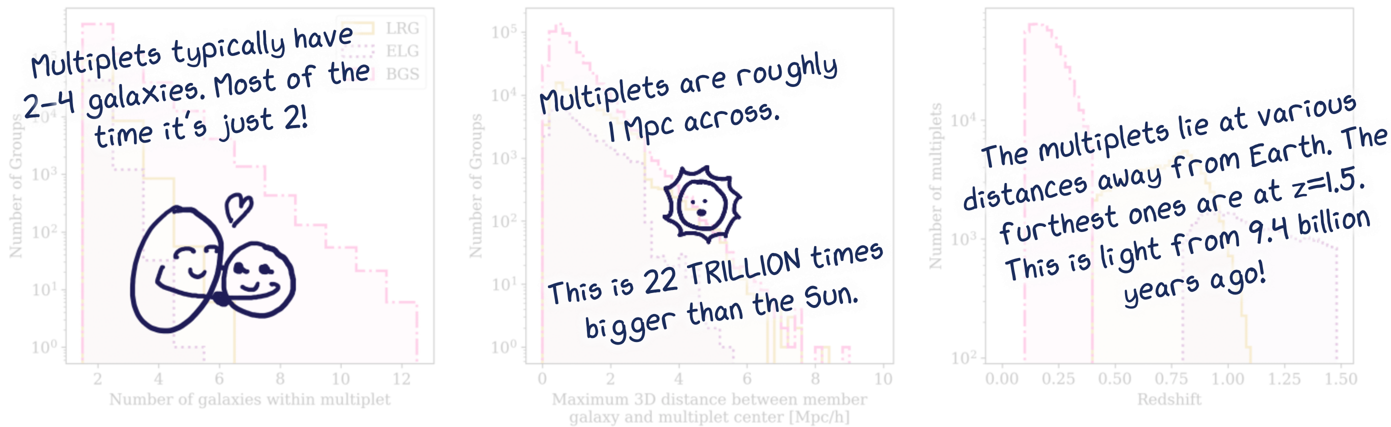

Figure 2. Demogr[illegible] composed of only two members, even for the densest sample, BGS, where 70% of multiplets are galaxy pairs. The spatial size of multiplets is shown in the middle panel, which is described by the maximum 3D distance betw[illegible] is a drop around 3 h^{-1}Mpc, corresponding to the maximum distance to the center for a pair of galaxies based on our multiplet definition (Section 3.1). The right panel shows the redshift distribution of multiplets.

These plots show information about the galaxy multiplets we find, which are described in the text below.

Galaxy type	Redshift Range	N galaxies	N galaxy multiplets	Volume [Gpc$^3h^{-3}$]
ELG	1.1 < z < 1.5	1.5 M	21 K	67.8
ELG	0.8 < z < 1.1	1.2 M	22 K	35.8
LRG	[illegible]	[illegible] M	[illegible] K	34.6
LRG	0.4 < z < 1.1	2.2 M	105 K	34.6
BGS	0.3 < z < 0.4	0.6 M	64 K	3.2
BGS	[illegible]	[illegible]	12 K	[illegible]
BGS	0.1 < z < 0.2	1.4 M	307 K	0.5
BGS Blue	0.1 < z < 0.2	0.56 M	81 K	0.5
BGS Red	0.1 < z < 0.2	0.54 M	100 K	0.5

Type of Galaxy — How far away they are — How dense the sample is

BGS: bright, nearby galaxies — "close" — very dense (brownie)

LRG: big elliptical galaxies — far away — less dense (cake)

ELG: faint spiral galaxies — REALLY far away — sparse (chocolate mousse)

Table 1. Properties of the DESI catalogues used to identify galaxy multiplets. The right column shows the comoving volume of the sample, estimated from the positions of gala[illegible] Blue and Red samples are described in Section 2.

We found multiplets using samples of many types of galaxies!

a $g-r$ colour greater than $0.5+3z$. The colour $g-r$ is computed [illegible] the galaxies' spectroscopic redshifts.

[illegible] DESI's survey selection and analysis rely on mock catalogues. These are generated with 25 N-body cosmological simulations from AbacusSummit (Hadzhiyska et al. 2021; Maksimova et al. 2021; Yuan et al. 2024). An important aspect of these is to [illegible] on thousands of objects at once via individually-controlled robotic positioners, which place fiber optic cables on galaxies. Their positions are limited to a set patrol radius and by proximity to other fibers, resulting in an under-sampling of highly clustered targets. Here we use the set of mock catalogues prepared for DESI Y1 clustering measurements, and two implementations of fiber assignment. The first [illegible] that targets are observed is simulated by running the fiber assignment algorithm with varying target priorities (Lasker et al. 2024). [illegible] the probability that galaxies are observed based on the number of survey [illegible] (...ni et al., in [illegible]

WHAT ARE MULTIPLETS AND HOW DO WE FIND THEM?

Multiplets are little sets of galaxies: as in a doublet, triplet, quadruplet, etc.

We find them by using the 3D positions of galaxies measured by DESI. The basic idea is to find the closest neighbor to each galaxy and then use an algorithm to identify sets within those connections.

3 ALIGNMENT METHOD

3.1 Identifying galaxy multiplets

Our measurement is a projected quantity, relating the orientation of multiplets in the plane of the sky as a function of transverse distance (Figure 1). However, we identify small multiplets of galaxies in 3D comoving space using spectroscopic redshifts. Each galaxy is matched to its nearest neighbour and all pairs are limited to a maximum separation in the plane of the sky r_p, and along the line of sight, $r_\parallel$. $r_\parallel$ is necessarily larger than r_p to account for the redshift-space distortions created by peculiar velocities of multiplet members. We then find multiplets within these matches using a Union Find algorithm to identify connected components within the graph of galaxy pairs (Galler & Fisher 1964). We set no maximum for the number of multiplet members. This is similar to the friends-of-friends algorithm used for identifying haloes in N-body simulations and for constructing group catalogues (Davis et al. 1985; Eke et al. 2004; Robotham et al. 2011). Note that unlike these catalogues, our goal is not to identify complete, gravitationally bound objects. We expect even nonviralized objects to contribute to our final measurement and so set no additional criteria such as completeness or velocity dispersion.

To explore the effectiveness of this algorithm to identify distinct multiplets, we created a catalogue of isolated multiplets, consisting only of multiplets where each member was a minimum of $2r_p$ and $2r_\parallel$ away from the nearest non-multiplet member. This had no significant effect on final results. We tested multiplets constructed from varying criteria, bet[illegible] $< r_\parallel < 12h^{-1}$Mpc. We found no significant effect on the amplitude of the final [illegible] cuts to max[illegible] model in Section 4. LRGs. For all samples, we use $r_p = 1.0h^{-1}$Mpc and $r_\parallel = 6.0$[illegible] such as scale cuts which depend on density or removing very close pairs (see Section 4.1) may improve the SNR and are worth exploring in future works.

We are careful to vary some of the algorithm parameters and make sure these choices don't impact our final results.

Properties of the DESI samples we identified multiplets in are shown in T[illegible] shown in Fig. 2. This displays the number of members within each multiplet, which is most often two. It also shows the spatial size of each mul-

This page shows information about the multiplets we find.

WHAT EXACTLY ARE WE MEASURING?

... ed by taking the maximum 3D distance between a multiplet member and the multiplet's centre in redshift space. Note that this can be greater than r_p and $r_{\parallel}$ since we only limit the distance between multiplet members, not its overall size.

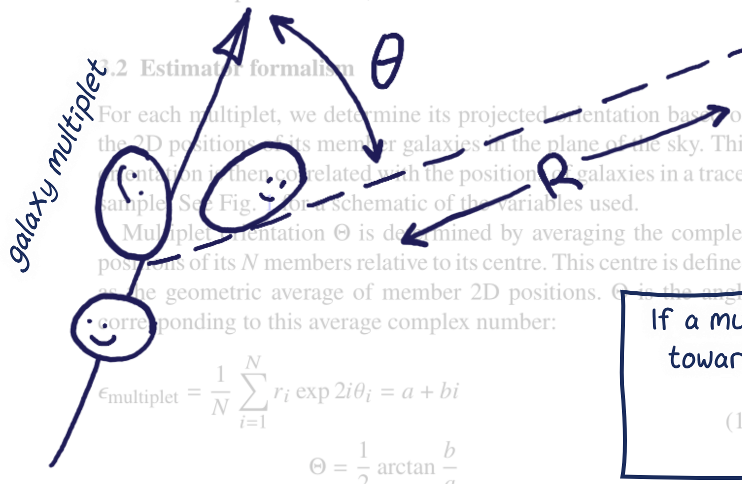

How do we measure correlations between multiplets and the cosmic web if the web is invisible?

Since galaxies cluster along the cosmic web, we can use other galaxies as "tracers" of the underlying dark matter.

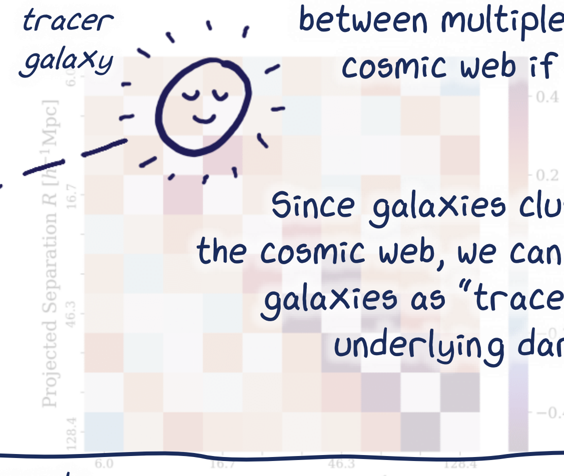

3.2 Estimator formalism

For each multiplet, we determine its projected orientation based on the 2D positions of its member galaxies in the plane of the sky. This orientation is then correlated with the positions of galaxies in a tracer sample. See Fig. ... for a schematic of the variables used.

Multiplet orientation Θ is determined by averaging the complex positions of its N members relative to its centre. This centre is defined as the geometric average of member 2D positions. Θ is the angle corresponding to this average complex number:

$$\epsilon_{\text{multiplet}} = \frac{1}{N}\sum_{i=1}^{N} r_i \exp 2i\theta_i = a + bi \tag{1}$$

$$\Theta = \frac{1}{2}\arctan\frac{b}{a}$$

If a multiplet points towards a tracer → $\theta = 0$ → $\cos(2\theta) = 1$

If multiplets have random orientations, on average: → $\cos(2\theta) = 0$

Figure 3. The reduced covariance matrix corresponding to the LRG signal ... has been subtracted ... There ... covariance in the multiplet alignment measurement between bins of projected separation, particularly in the largest bins.

For each member i, r_i is the projected distance to the multiplet centre ... to the centre. We do not consider the full ellipticity of the multiplet, i.e. axis ratio, because ... meaningless for multiplets with two members and it is not expected to increase our signal-to-noise ratio. For single galaxies, measurements with the SDSS-III BOSS LOWZ sample have found ... 2015). We find a similar result with DESI Year 1 LRGs and Legacy Imaging (Fig. 9).

Our measurement comes down to two numbers:

1. The orientation of a multiplet relative to a tracer, θ
2. The distance between a multiplet and a tracer, R

This orientation angle is then measured relative to the tracer sample. In most cases, the tracer sample is the same as the one used to identify multiplets. For each pair, consisting of a galaxy multiplet and ... the difference between the position angle of the multiplet relative to the tracer, ϕ, and the multiplet's orientation:

We find millions of multiplet-tracer pairs and find the average orientation as a function of separation. (2)

The relevant quantity is $\cos(2\theta)$ as a function of the projected separation between the multiplet and the tracer, R. This is then averaged over every multiplet-tracer pair. This is similar to conventions in intrinsic alignments and ensures the relative angle is invariant under rotation. Since we are mostly measuring the orientation of a pair of galaxies ... to a squeezed three-point correlation function. For multiplets with more than two members, the pair of points describe the N-weighted orientation.

We expect that **multiplets will "point" towards areas of high density**, as traced by other galaxies. And that the effect will be strongest when a multiplets is close to a tracer.

Just like long galaxies!

The code for these measurements, and other analysis throughout the paper, is available in the repository spec-IA.

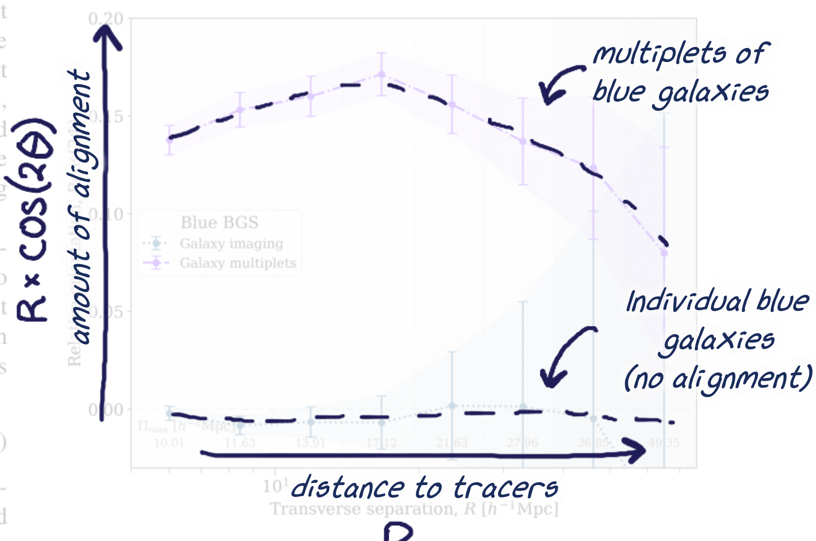

Figure 4. A demonstration of the advantages of using multiplet alignment. Here we show the tidal alignment of galaxy and multiplet orientations within a dense, blue sample. The alignment of ... galaxies is highly sensitive to ... alignment of multiplets displays a clear signal.

Why so blue??
Here we show how we can detect a correlation to the cosmic web using multiplets of blue galaxies. This is much better than the alignment of individual blue galaxies, which is 0.

3.3 Measurement

When measuring the projected orientation of multiplets relative to a tracer catalogue, we limit the multiplet-tracer pairs to a line-of-sight separation that is unique to each bin of projected separation, $\Pi_{\max}(R_{\text{bin}})$. This is to maximise the signal-to-noise of our measurement. In the case of positive tidal alignment, shapes are elongated along the stretching direction of the tidal field. In this situation, the ... measurable orientation in the plane of the sky. Therefore, multiplet-tracer pairs that are close in the plane of the sky but distant along the line-of-sight direction will ...

signal. At la... contribution from radially distant galaxies and it becomes advantageous to increase $\Pi_{\max}$. We chose $\Pi_{\max}(R_{\text{bin}}) = 6h^{-1}\text{Mpc} + \frac{2}{3}R_{\text{bin}}$ based on the signal-to-noise ratio of our final LRG signal. Our model estimate is computed in these same R bins. Throughout plots in this paper, the varying values of $\Pi_{\max}$ are shown through shaded regions and marked explicitly. We use this projected statistic, as opposed to keeping the measurement as a function of r_p and $r_{\parallel}$, because most of the signal is along the LOS for tidal alignments due to the projection of shapes. Additionally, a projected statistic allows for more direct modelling as it is less sensitive to redshift-space distortions (Figure 7).

For each measurement, we separate the multiplet catalogue into 100 sky regions by right ascention and declination, with equal num...

WHAT ARE THE MEASUREMENTS?

The measurements are.... on the next page! But there's a sneak-peak here.

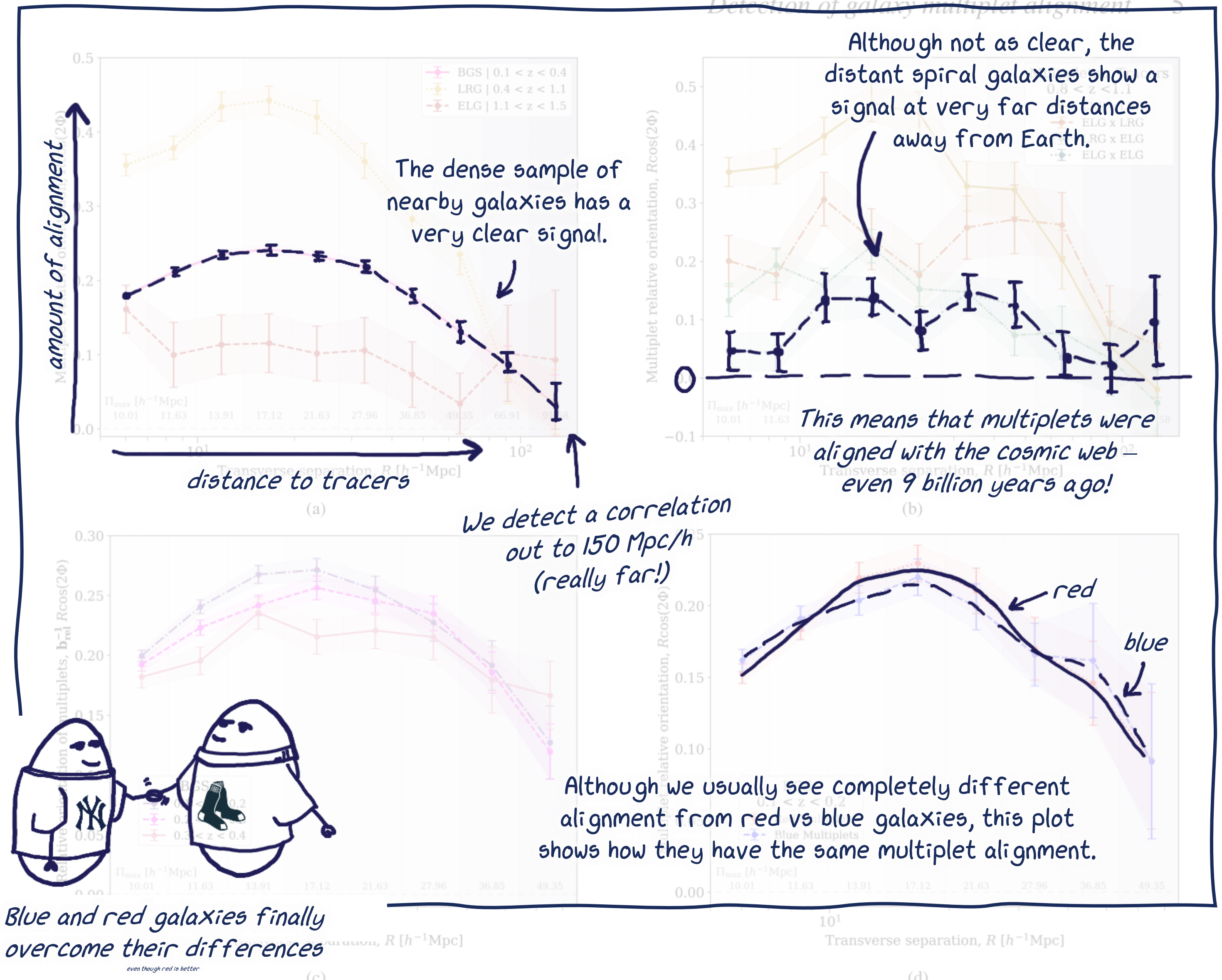

These plots are the result of us playing around and making this measurement with many types of galaxies. Here I've highlighted a few interesting results.

Our measurements reveal that multiplets are indeed aligned with the cosmic web!!

And these correlations happen even at 150 Mpc/h, i.e. the size of the largest structures in the universe.

This is so far away that it's hard to come up with a sensible comparison.

So I won't try. This distance is equal to 10^{24} alligators laid end-to-end. Together they would weigh 10x more than the Earth.

This shows that tiny groups of galaxies still remember the cosmic web connected to their formation in the early universe.

Now onto the hard part, interpreting the measurements...

WHAT DOES ALL THIS MEAN?

The rest of our paper explores what is actually happening in the universe to create these correlations. Our goal is to quantitatively connect our measurements to the cosmic web.

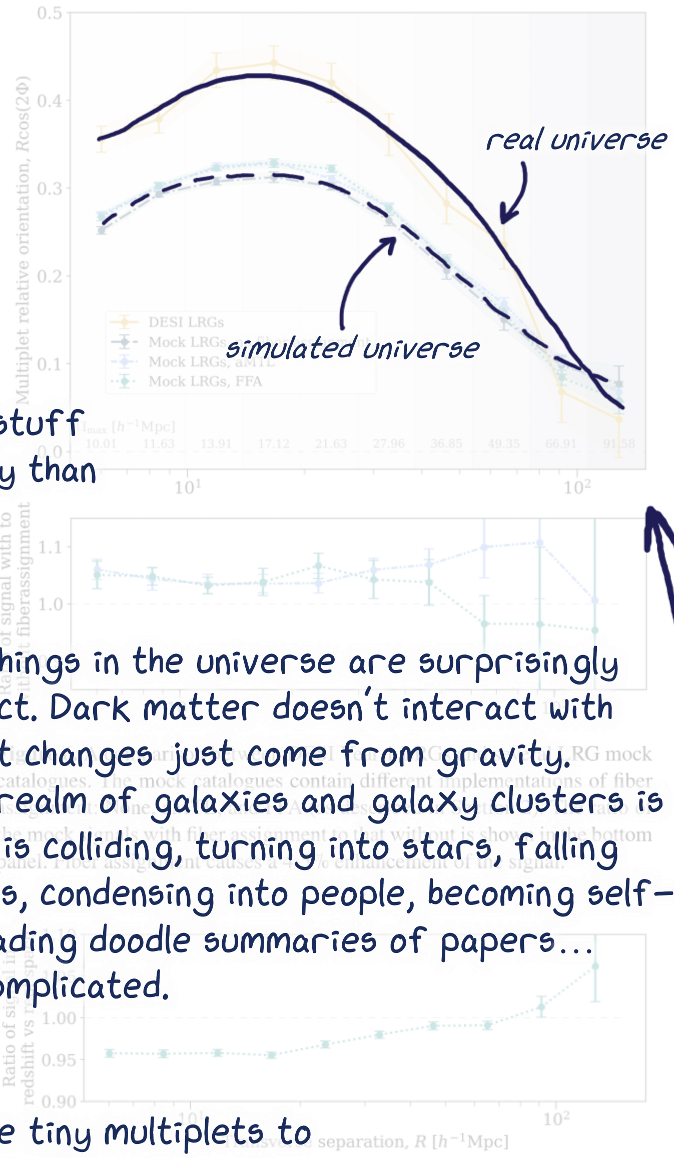

A challenging part of this is that stuff on small scales behaves differently than stuff on large scales.

The biggest things in the universe are surprisingly easy to predict. Dark matter doesn't interact with itself, so most changes just come from gravity. However, the realm of galaxies and galaxy clusters is messy. Stuff is colliding, turning into stars, falling into black holes, condensing into people, becoming self-aware and reading doodle summaries of papers... It's all very complicated.

To cosmologists, galaxies are just lil' guys

So how do we connect these tiny multiplets to the largest structures in the universe?

COMPARING TO SIMULATIONS

Our first step is to see what the alignment of multiplets looks like in simulated universes.

We are measuring things on big scales, so typically these simulations work just fine. However, we find that multiplet correlations in the simulated universe are lower than in the real universe!

The simulations we use are designed to reproduce statistics about the universe on very large scales. So they only include dark matter.

You shouldn't always trust computers....

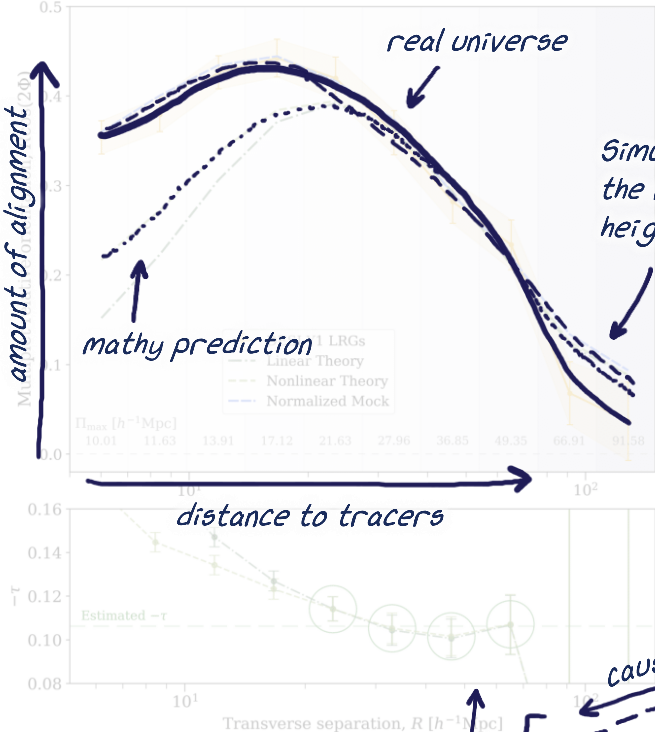

Figure 8. Comparison between the LRG multiplet alignment and the model predictions using both a linear and nonlinear matter power spectrum. These model predictions have been normalized using a τ [illegible] estimated from the bin measurements circled in the bottom panel. We also show a normalized measurement of the multiplet alignment made with [illegible] aMTL mock catalogues (Section 4.1), which sufficiently reproduces the signal shape on these scales.

The shape of our measurement is a result of the big stuff – cosmic web. The amplitude is a result of the small stuff – how galaxies move around each other.

removing some of this dilut[illegible] separation of the initial pairs [illegible] LRG multiplet catalogue to $r_p > 0.5h^{-1}$Mpc and find a similar enhancement of the signal, 10% between 6 – 60 h^{-1}Mpc. This may be a useful addition to future studies of multiplet alignment.

We do not include the effects of RSD in our analytic model (Section 4), so to test this assumption we reproduce the aMTL measurement in real space. Here, galaxy multiples are still found in redshift space, but the multiplet-tracer correlations are measured using the true positions of the multiplet centres and tracers. The effects of RSD on the tracer catalogue appear to make a 0 – 5% difference on scales beyond 10 h^{-1}Mpc (Fig. 7).

INTERPRETATION WITH MATH

4.2 Modeling

To quantify the connection between multiplet orientation and the underlying matter distribution, we assume a linear relationship between shapes [illegible] trinsic alignment assumes the ellipticity of objects are linearly related to the gravitational potential, which is described by either the linear (LA) [illegible] 2007; Hirata et al. 2007). The latter is often used for individual LRGs [illegible] et al. [illegible] measurements.

Following the convention in [illegible]

Besides simulations, we can also use math! Here we model the 3D gravitational field created by large-scale structure and then derive an equation which describes how different components in the universe combine to produce our measurement.

describe the traceless tidal tensor as

$$T_{ij} = \partial_i \partial_j \phi - \frac{1}{3}\delta^{\rm K}_{ij}\nabla^2\phi, \quad (3)$$

where $\nabla^2\phi \propto \delta$ is given by the Poisson equation, with δ being the fractional overdensity. Constants are absorbed into the unmodeled amplitude of the correlation. $\delta^{\rm K}_{ij}$ is the Kronecker delta. In Fourier space this is expressed as

$$T_{ij}(\vec{r}) = \int \frac{d^3k}{(2\pi)^3}\left(\frac{k_i k_j - \frac{1}{3}\delta^{\rm K}_{ij}k^2}{k^2}\right)\tilde{\delta}_m(\vec{k})e^{i\vec{k}\cdot\vec{r}}, \quad (4)$$

where we have use $\tilde{\delta}$ to indicate a variable in Fourier space. Our measured signal is a projected quantity, where we define $\hat{z}$ to be along the line-of-sight. Therefore, for a projection with $\alpha, \beta = \{x, y\}$ and using the relation $T_{xx} + T_{yy} = -T_{zz}$, the relevant projection of the tidal field is $(T_{\alpha\beta} + T_{zz}/2)$.

In this study we characterize the relevant "shapes" of objects solely by orientation, instead of the full ellipticity. This axis-ratio component of shapes affects the amplitude of the signal as does any systematic misalignment of galaxy multiplets to the large-scale field caused by local dynamics. Our focus in this work is to explore how multiplet alignment traces the tidal field across large scales, without making any assumptions about the effect's amplitude. Therefore, we fold in the full ellipticity information and any misalignment effects into the signal amplitude, assuming neither display scale dependence at large separations. This is similar to the "stick model" employed for describing the positions and alignments of galaxies within haloes (Fortuna et al. 2021; Schneider & Bridle 2010).

The projected ellipticity of galaxy multiplets can be described by the traceless tensor

$$\epsilon_{\alpha,\beta} = \tau(T_{\alpha\beta} + \frac{1}{2}T_{zz}). \quad (5)$$

[illegible] orientation of the galaxy multiplets, as defined in Section 3.2, and τ is a parameterization of the shape's response to the tidal field. τ includes any effects from the full-shape information and any misalignment of shapes relative to the tidal direction. The full complex ellipticity is described as

$$\epsilon = \tau[T_{xx} - T_{yy} + 2iT_{xy}]. \quad (6)$$

The quantity of interest is the expectation value of the cross-correlation between projected shapes and the matter field, Q:

$$\mathcal{E}_{\rm model} = \frac{1}{2}\langle \epsilon^* Q + \epsilon Q^* \rangle. \quad (7)$$

We describe the 3D matter field in a particular bin of transverse separation $R_{\rm bin}$ and line-of-sight separation $\pm\Pi_{\rm max}$ as

$$Q(R_{\rm bin}, \pm\Pi_{\rm max}) = \frac{\int d^3r W(\bar{r})\delta_g e^{2i\theta_r}}{\int d^3r W(\bar{r})(1+\xi_{\epsilon g})}. \quad (8)$$

Here, δ_g is the fractional matter overdensity, $\xi_{\epsilon g}$ is the shape orientation – galaxy correlation function, r is the 3D separation, and θ_r is the 3D relative angle. $W(\bar{r})$ is a function representing the bin selection, both an annulus in R and $\pm$[illegible] $\bar{r}$ is used to denote a binned quantity. The expansion of $\epsilon^* Q + \epsilon Q^*$ can be found in Appendix A, and re[illegible]

$$\mathcal{E}_{\rm model} = \frac{-\tau}{\int d^3r W(\bar{r})(1+\xi_{\epsilon g})} \int d^3r W(\bar{r}) [\text{illegible}] \quad (9)$$
$$\int \frac{dk_z}{2\pi} \int K dK J_2(KR)\frac{K^2}{k^2}P_{gm}(k)e^{ik_z z},$$

where J_2 is the second Bessel function of the first kind and $P_{gm}(k)$

This is not easy to do or explain, but I'll break down the final equation on the next page.

is the galaxy-matter power spectrum. k represented 3D position in Fourier space, K represents the 2D position on the plane of the sky (k_x, k_y), and k_z lies along the line of sight. $k^2 = K^2 + k_z^2$.

The remainder of this Section describes how we compute Equation 9, by breaking it into the components we measure or calculate. Beginning with the denominator,

$$\int d^3 r W(\bar{r})(1 + \xi_{\epsilon g}) = \pi (R_{\max}^2 - R_{\min}^2)(2\Pi_{\max} + \bar{w}_p).$$

$\bar{w}_p$ is the integrated 2-point cross-correlation function between the multiplet and tracer catalogue, $w_p(R)$, within an annulus of $R_{\min}$ and $R_{\max}$:

$$\bar{w}_p(R_{\rm bin}) = \frac{1}{\pi(R_{\max}^2 - R_{\min}^2)} \int_{R_{\min}}^{R_{\max}} 2\pi R dR w_p(R). \quad (11)$$

We further define $\mathcal{J}_2$, a binned version of the second Bessel function integrated over a given $R_{\rm bin}$:

$$\mathcal{J}_2(K) = \frac{2}{(R_{\max}^2 - R_{\min}^2)} \int_{R_{\min}}^{R_{\max}} R dR J_2(KR), \quad (12)$$

This can be solved analytically (Equation A8). Using the relation

$$\frac{1}{2\Pi_{\max}} \int_{-\Pi_{\max}}^{\Pi_{\max}} dz e^{ik_z z} = \mathrm{sinc}(k_z \Pi_{\max}), \quad (13)$$

we further define an expression of the relevant matter distribution for a given $\Pi_{\max}$:

multiplet orientation
(the signal we measure)

$$\mathcal{P}_\Pi(K) = 2\Pi_{\max} \int \frac{dk_z}{2\pi} \frac{K^2}{K^2 + k_z^2} b_g P_{gm}\left(\sqrt{K^2 + k_z^2}\right) \mathrm{sinc}(k_z \Pi_{\max}). \quad (14)$$

In practice, for this we use the matter power spectrum and galaxy bias $b_g P_{mm}(k)$, with $b_g = 1.99$ for DESI LRGs (Mena-Fernández et al. 2024). Combining these expressions, the model prediction for our signal $\mathcal{E}(R)$ is simplified to

$$\mathcal{E}_{\rm model}(R) = \frac{-\tau}{(2\Pi_{\max} + \bar{w}_p)} \int K dK \mathcal{J}_2(K, R) \mathcal{P}_\Pi(K). \quad (15)$$

$$\mathcal{E} = \frac{-\tau}{(2\Pi_{\max} + \bar{w}_p)} \int K dK J_2(KR) P_\Pi(K)$$

the variable which describes small-scale effects, or the extent to which a multiplet responds to the exterior gravitational forces

adjustment for how clustered galaxies are

gravitational force created by the cosmic web

We compute this numerically in bins of $(R_{\min}, R_{\max})$ with the corresponding $\Pi_{\max}$ value in each. The model prediction made with both a linear and nonlinear matter power spectrum can be seen in Fig. 8. The power spectra are from AbacusSummit and evaluated at $z = 0.8$. We normalize the models by taking their ratio to the large-scale signal, using the points circled in the lower panel of Figure 8. This results in an estimate τ for the LRG multiplets of -0.106 ± 0.002 for both LA and NLA. We find that these models can sufficiently match the shape of our measurement only down to scales of 20 h^{-1}Mpc, while the LRG mock catalogue matches below 10 h^{-1}Mpc. The corresponding τ value for this mock is also -0.106 ± 0.002. Therefore the NLA model is sufficient for very large scales, but fails to capture the non-linear dynamics between multiplets and tracers in the way that an N-body simulation can.

The alignment amplitude is often characterized with $A_{\rm IA}$ (Catelan & Porciani 2001; Hirata & Seljak 2004; Blazek et al. 2015). $A_{\rm IA}$ describes the relationship between intrinsic galaxy shear, γ_{ij}^I, with the tidal tensor, T_{ij}, as defined in Eq. 3. In the case of "early alignment", it is assumed that shapes are aligned at time of formation and then evolve with the matter field.

$$\gamma_{ij}^I = -A_{\rm IA}(z) C_1 \frac{\rho_{\rm m,0}}{D(z)} T_{ij} \quad (16)$$

Here, $\rho_{\rm m,0}$ is the matter density, $D(z)$ is the growth factor, normalized so $\bar{D}(z) = (1+z)D(z)$ is unity at matter domination, and C_1 is a

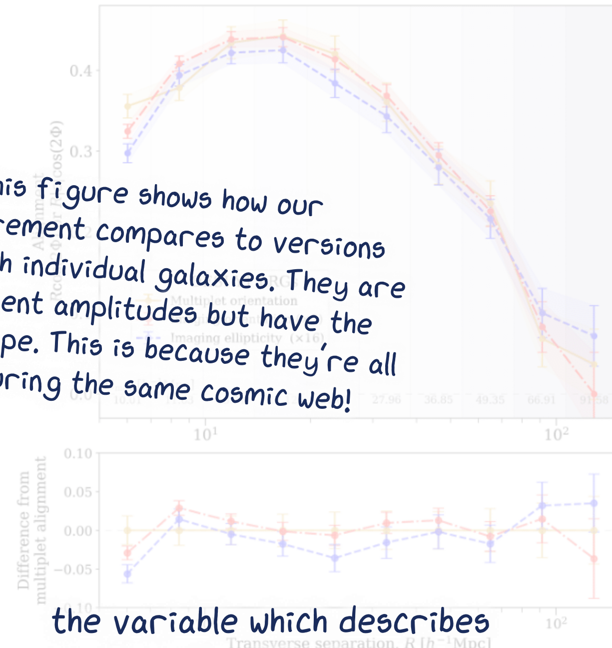

Figure 9. Here we compare the alignment of galaxy multiplets to the alignment of individual galaxies within the DESI LRG sample. The yellow line shows the alignment of the orientations of LRG multiplets relative to positions of full sample (Section 3.3). The red line is the orientations of individual LRGs relative [illegible] for an easier comparison. These two measurements model shapes as "sticks", described only by orientation. The blue line is the full shape alignment of LRGs, taking into account galaxy axis ratio and multiplied by 16 comparison. The bottom panel shows the difference in the points plotted above, highlighting the similar scale-dependence of each estimator. The average signal-to-noise for each of these measurements shown is 9.2 [illegible] for imaging, and 11.0 for imaging with ellipticity. These measurements were made with 105 thousand multiplets and 2.2 million individuals LRGs.

historical normalization constant of $5 \times 10^{-14} M_\odot^{-1} h^{-2}$ Mpc^3 (Brown et al. 2002). The relationship to our alignment amplitude τ is

$$A_{\rm IA}(z) = -\frac{\tau}{C_1} \frac{D(z)}{\rho_{\rm m,0}} \quad (17)$$

For our "stick" model of LRG multiples, this corresponds to an average value of $A_{\rm IA} = 5.7 \pm 0.1$. For reference, the corresponding stick alignment of the same sample using individual galaxies and Legacy Survey Imaging is $A_{IA} = 1.96 \pm 0.001$, about 5 times higher than when using the full-shape information (Fig. 9). For this measurement we use the ellipticity definition

$$\epsilon_+ = \frac{a - b}{a + b} \cos 2\theta, \quad (18)$$

based on the galaxy major and minor axis, a and b, and orientation, θ.

Fig. 9 is also a useful demonstration of how, although very different amplitudes, the alignment of multiplet orientation has the same scale dependence of shape alignment and can be modeled similarly. Additionally, mutliplet alignment produces a comparable signal-to-noise measurement as full shape alignment, with less than 5% of the objects. While multiplet alignment does not necessarily outperform individual galaxies within the LRG sample, it is promising for denser regions or samples that show weaker intrinsic galaxy alignment.

CONCLUSIONS

5 CONCLUSION

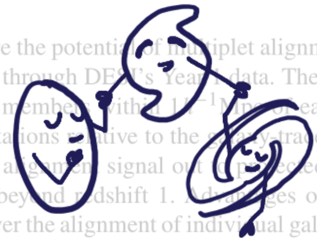

The orientations of tiny groups of galaxies, or "multiplets", trace out the largest structures in the universe.

In this work we explore the potential of multiplet alignment for large spectroscopic surveys through DESI's Year 1 data. These multiplets mostly consist of 2-4 members within 1 h^{-1}Mpc of each other. By measuring their orientations relative to the galaxy-traced tidal field, we detect an intrinsic alignment signal out to projected separations of 100 h^{-1}Mpc and beyond redshift 1. Advantages of this galaxy multiplet alignment over the alignment of individual galaxies depend on properties of the galaxy catalogue, including morphology, density, and imaging quality. We find similar signals regardless of galaxy colour or luminosity, which is a promising result for measuring the tidal field with galaxy populations that typically display little or no intrinsic shape alignment.

We come up with a way to describe these correlations and make measurements using samples of different types of galaxies.

Using the LRG sample as a case study, we reproduce the LRG [illegible] body simulations, finding they under-predict the signal amplitude but match its shape. Using a nonlinear tidal alignment model, we find an amplitude parameter $\tau = -0.106 \pm 0.002$, which characterizes the response of multiplet orientations to the tidal field. This modelling matches the measured signal above scales of $20h^{-1}$Mpc but fails to capture nonlinear effects at smaller scales, unlike the N-body prediction.

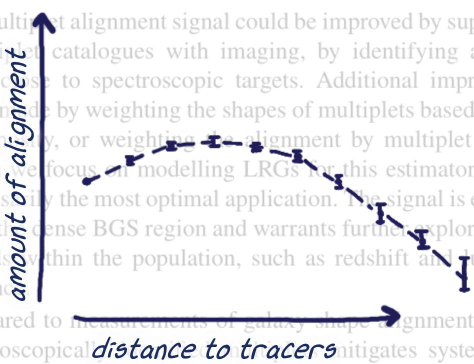

The multiplet alignment signal could be improved by supplementing multiplet catalogues with imaging, by identifying additional galaxies close to spectroscopic targets. Additional improvements could be made by weighting the shapes of multiplets based on member luminosity, or weighting the alignment by multiplet richness. Although we focus on modelling LRGs for this estimator, they are not necessarily the most optimal application. The signal is especially clear for the dense BGS region and warrants further exploration into sub-trends within the population, such as redshift and luminosity dependence.

Compared to measurements of galaxy shape alignments, the use of spectroscopical[illegible] mitigates systematic effects from imaging and shape measurements, and can extend intrinsic alignment studies to samples that do not display intrinsic shape alignments (Fig. 4). The remaining 4 years of the DESI survey will significantly increase the size and comoving density of the ELG sample, allowing for better measurements of intrinsic alignment at higher redshifts.

Unlike the orientations of individual galaxies, our method can be applied to any galaxy type and doesn't rely on good pictures of galaxies. This could be a new way to map out the large-scale structures of the universe. It would require understanding the small effects or calibrating the amplitude of our signal. We have a few ideas for how to do this!

Although we describe multiplets as distinct objects throughout this work and model their orientations with intrinsic alignment con[illegible] dark matter halo shapes. The multiplet alignment estimator is es[illegible] cases the orientation of the galaxy pair is determined by all nearby [illegible] squeezed limit is coupled to the linear tidal field. This indicates that there is a [illegible] of nonlinear collapse preserved even into the non-linear regime, at the scales of the multiplet sizes of around 1 h^{-1}Mpc.

In principle, this measurement can be used to produce an intrinsic shear map and reconstruct the underlying matter field. Unlike the shear measurements from weak lensing, intrinsic shear preserves line-of-sight information. However, [illegible] will be i[illegible]ts from the foreground mass on the multiplet shape polarization and therefore any inference of the tidal field. An advantage of using galaxy multiples to [illegible] estimator has systematics that are distinct from the galaxy field, and may provide an avenue to more precisely measure large-scale modes.

The next few years of DESI will fill out more gaps in our map of the universe – using galaxies that are especially well-suited for measuring multiplet alignment.

The difficulty lies in determining the modelling amplitude, $\tau(z)$. This could potentially be determined through hydrodynamic simulations or by calibrating τ with a weak lensing map and an assumed amplitude of the redshift-dependent matter power spectra. Such a mass [illegible] the underlying cosmological dependence. With the right sample and understanding of the modelling amplitude, this could be a unique way to explore the large-scale matter field in future surveys.

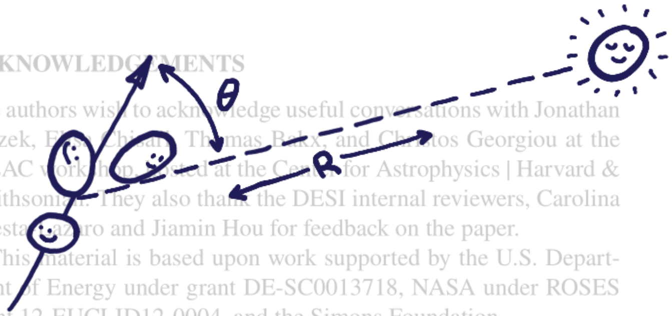

The shape of the resulting measurement is a result of the underlying cosmic web, and is the same regardless of what types of galaxies we use. We can predict this shape using simulations of dark matter.

The height of the measurement is a result of smaller effects: how galaxies move around each other in the little groups. This part is harder to model.

ACKNOWLEDGEMENTS

The authors wish to acknowledge useful conversations with Jonathan Blazek, [illegible], Thomas Bakx, and Christos Georgiou at the LILAC workshop, hosted at the Center for Astrophysics | Harvard & Smithsonian. They also thank the DESI internal reviewers, Carolina Cuesta-Lazaro and Jiamin Hou for feedback on the paper.

This material is based upon work supported by the U.S. Department of Energy under grant DE-SC0013718, NASA under ROSES grant 12-EUCLID12-0004, and the Simons Foundation.

This material is based upon work supported by the U.S. Department of Energy (DOE), Office of Science, Office of High-Energy [illegible] tional Energy Research Scientific Computing Center, a DOE Office of Science User Facility under the same contract. Additional support for [illegible], Division of Astronomical Sciences under Contract No. AST-0950945 [illegible] of the United Kingdom; the Gordon and Betty Moore Foundation; the Heising-Simons Foundation; the French Alternative Energies and Atomic Energy Commission (CEA); the National Council of Science and Technology of Mexico (CONACYT); the Ministry of Science and In[illegible]tions: https://www.desi.lbl.gov/collaborating-institutions.

The DESI Legacy Imaging Surveys consist of three individual [illegible] k Energy Camera Legacy Survey (DECaLS), the Beijing-Arizona Sky Survey (BASS), and the Mayall z-band Legacy Survey (MzLS). DECaLS, BASS and MzLS together include data obtained, respectively, at the Blanco telescope, Cerro Tololo Inter-American Observatory, NSF's NOIRLab; the Bok telescope, Steward Observatory, University of Arizona; and the Mayall telescope, Kitt Peak National Observatory, NOIRLab. NOIRLab is [illegible] the Association of Universities for Research in Astronomy (AURA) under a cooperative agreement with the National Science Foundation. Pipeline processing and analyses of the data [illegible] NOIRLab and the Lawrence Berkeley National Laboratory. Legacy Surveys also uses data products from the Near-[illegible] Infrared Survey Explorer (NEOWISE), a project of the Jet Propulsion Laboratory/California Institute of Technology, funded by the National Aeronautics and Space Administration. Legacy Surveys was supported by: the Director, Office of Science, Office of High Energy Physics of the U.S. Department of Energy; the National Energy Research Scientific Computing Center, a DOE Office of Science User Facility; the U.S. National Science Foundation, Division of Astronomical Sciences; the National Astro[illegible] of Sciences and the Chinese National Natural Science Foundation. LBNL is managed by the Regents of the University of California under contract to [illegible] mplete acknowledgments can be found at https://www.legacysurvey.org/.

Any opinions, findings, and conclusions or recommendations ex-

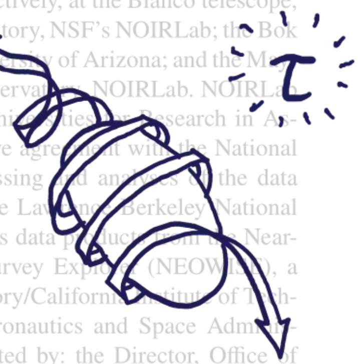

But wait, there's (always) more!

Our acknowledgement section is as long as the conclusions! It takes the support of many organizations and people to make a big survey like DESI possible.

pressed in this material are those of the author(s) and do not necessarily reflect the views of the U.S. National Science Foundation, the U. S. Department of Energy, or any of the listed funding agencies.

The authors are honored to be permitted to conduct scientific research on Iolkam Du'ag (Kitt Peak), a mountain with particular significance to the Tohono O'odham Nation.

SEE THE DATA YOURSELF

DATA AVAILABILITY

You can find the publicly available data we used here

The DESI Legacy Imaging Survey is publicly available at legacysurvey.org. DESI data is available at data.desi.lbl.gov/doc/releases/edr/. Iron covers the DESI Year 1 sample and will be released as part of DESI Data Release 1 (DR1) (DESI Collaboration 2025). AbacusSummit simulations are available at abacusnbody.org.

Data plotted in this paper can be downloaded from zenodo.org/records/13230864.

PAPERS WE REFERENCE

REFERENCES

Our work is one more step in a long line of papers building on each other!

These papers are all * OFFICIAL * papers about the DESI Survey

A. Ross et al. 2024, in preparation
Akitsu K., Kurita T., Nishimichi T., Takada M., Tanaka S., 2021, Physical Review D, ...
Akitsu K., Li Y., Okumura T., 2023, Physical Review D, 107, 063531
Blazek J., ... Journal of Cosmology and Astroparticle Physics, 201..., 015
Bridle S., King L., 2007, New Journal of Physics, 9, 444
Brown M. L., Taylor A. N., Hambly N. C., Dye S., 2002, Monthly Notices of the Royal Astronomical Society, 333, 501
Catelan P., Porciani C., 2001, Monthly Notices of the Royal Astronomical Society, 323, 713
Chisari N. E., Dvorkin C., 2013, Journal of Cosmology and Astroparticle Physics, 12, 029
DESI Collaboration 2024, in preparation
DESI Collaboration 2025, in preparation
DESI Collaboration et al., 2016b, The DESI Experiment Part I: Science,Targeting, and Survey Design, doi:10.48550/arXiv.1611.00036, https://ui.adsabs.harvard.edu/abs/2016arXiv161100036D
DESI Collaboration et al., 2016a, The DESI Experiment Part II: Instrument Design, https://ui.adsabs.harvard.edu/abs/2016arXiv161100037D
DESI Collaboration et al., 2022, The Astronomical Journal, 164, 207
DESI Collaboration et al., 2023a, The Early Data Release of the Dark Energy Spectroscopic Instrument, doi:10.48550/arXiv.2306.06308, https://ui.adsabs.harvard.edu/abs/2023arXiv230606308D
DESI Collaboration et al., 2023b, Validation of the Scientific Program for the Dark Energy Spectroscopic Instrument, doi:10.48550/arXiv.2306.06307, https://ui.adsabs.harvard.edu/abs/2023arXiv230606307D
DESI Collaboration et al., 2024a, arXiv e-prints, p. arXiv:2404.03000
DESI Collaboration et al., 2024b, arXiv e-prints, p. arXiv:2404.03001
DESI Collaboration et al., 2024c, arXiv e-prints, p. arXiv:2404.03002
Dark Energy Survey and Kilo-Degree Survey Collaboration et al., 2023, The Open Journal of Astrophysics, 6, 36
Davis M., Efstathiou G., Frenk C. S., White S. D. M., 1985, The Astrophysical Journal, 292, 371
Dey A., et al., 2019, The Astronomical Journal, 157, 168
Eke V. R., et al., 2004, Monthly Notices of the Royal Astronomical Society, 348, 866
Fortuna M. C., Hoekstra H., Joachimi B., Johnston H., Chisari N. E., Georgiou C., Mahony C., 2021, Monthly Notices of the Royal Astronomical Society, 501, 2983
Galler B. A., Fisher M. J., 1964, Commun. ACM, 7, 301
Georgiou C., et al., 2019, Astronomy and Astrophysics, 622, A90
Georgiou C., Bakx T., van Donkersgoed J., Chisari N. E., 2023, ... future surveys, doi:10.48550/arXiv.2309.03841, https://ui.adsabs.harvard.edu/abs/2023arXiv230903841G
Guy J., et al., 2023, The Astronomical Journal, 165, 144
Hadzhiyska B., Eisenstein D., Bose S., Garrison L. H., Maksimova N., 2021, Monthly Notices of the Royal Astronomical Society, 509, 501
Hahn C., et al., 2023, The Astronomical Journal, 165, 253
Hirata C. M., Seljak U., 2004, Physical Review D, 70, 063526
Hirata C. M., Mandelbaum R., Ishak M., Seljak U., Nichol R., Pimbblet K. A., Ross N. P., Wake D., 2007, Monthly Notices of the Royal Astronomical Society, 381, 1197
Joachimi B., et al., 2015, Space Science Reviews, 193, 1
Krolewski A., et al., 2024, Impact and mitigation of spectroscopic systematics on DESI DR1 clustering measurements, doi:10.48550/arXiv.2405.17208, https://ui.adsabs.harvard.edu/abs/2024arXiv240517208K
Kurita T., Takada M., 2023, Physical Review D, 108, 083533
Lamman C., Tsaprazi E., Shi J., Niko Šarčević N., Pyne S., Legnani E., Ferreira T., 2023a, The IA Guide: A Breakdown of Intrinsic Alignment Formalisms, doi:10.48550/arXiv.2309.08605, https://ui.adsabs.harvard.edu/abs/2023arXiv230908605L
Lamman C., et al., 2023b, Monthly Notices of the Royal Astronomical Society, 522, 117
Lamman C., et al., 2024, Monthly Notices of the Royal Astronomical Society, 528, 6559
Lasker J., et al., 2024, Production of Alternate Realizations of DESI Fiber Assignment for Unbiased Clustering Measurement in Data and Simulations, doi:10.48550/arXiv.2404.03006, https://ui.adsabs.harvard.edu/abs/2024arXiv240403006L
Lee J., Ryu S., Baldi M., 2023, The Astrophysical Journal, 945, 15
Levi M., et al., 2013, The DESI Experiment, a whitepaper for Snowmass 2013, doi:10.48550/arXiv.1308.0847, https://ui.adsabs.harvard.edu/abs/2013arXiv1308.0847L
Maksimova N. A., Garrison L. H., Eisenstein D. J., Hadzhiyska B., Bose S., Satterthwaite T. P., 2021, Monthly Notices of the Royal Astronomical Society, 508, 4017
Mena-Fernández J., et al., 2024, HOD-Dependent Systematics for Luminous Red Galaxies in the DESI 2024 BAO Analysis, doi:10.48550/arXiv.2404.03008, https://ui.adsabs.harvard.edu/abs/2024arXiv240403008M
Miller T. N., et al., 2023, The Optical Corrector for the Dark Energy Spectroscopic Instrument, doi:10.48550/arXiv.2306.06310, https://ui.adsabs.harvard.edu/abs/2023arXiv230606310M
Myers A. D., et al., 2023, The Astronomical Journal, 165, 50
Okumura T., ... 2009, ..., 694, L30 ... 45, L30
Okumura T., Taruya A., Nishimichi T., 2019, Physical Review D, 100, 103507
Oppenheimer B. D., Babul A., Bahé Y., Butsky I. S., McCarthy I. G., 2021, Universe, 7, 209
Philcox O. H. E., Slepian Z., Hou J., Warner C., Cahn R. N., Eisenstein D. J., 2022, Monthly Notices of the Royal Astronomical Society, 509, 2457
Raichoor A., et al., 2023, The Astronomical Journal, 165, 126
Robotham A. S. G., et al., 2011, Monthly Notices of the Royal Astronomical Society, 416, 2640
Saga S., Shiraishi M., Akitsu K., Okumura T., 2024, Physical Review D, 109, 043520
Schlafly E. F., et al., 2023, The Astronomical Journal, 166, 259
Schneider M. D., Bridle S., 2010, Monthly Notices of the Royal Astronomical Society, 402, 2127
Shi J., et al., 2024, Monthly Notices of the Royal Astronomical Society, 528, 1487
Singh S., Mandelbaum R., 2016, Monthly Notices of the Royal Astronomical Society, 457, 2301
Singh S., Mandelbaum R., More S., 2015, Monthly Notices of the Royal Astronomical Society, 450, 2195
Slepian Z., Eisenstein D. J., 2015, Monthly Notices of the Royal Astronomical Society, 454, 4142
Slepian Z., et al., 2017, Monthly Notices of the Royal Astronomical Society,

469, 1738

Smargon A., Mandelbaum R., Bahcall N., Niederste-Ostholt M., 2012, Monthly Notices of the Royal Astronomical Society, 423, 856

Sunayama T., 2023, Monthly Notices of the Royal Astronomical Society, 521, 5064

Troxel M. A., Ishak M., 2015, Physics Reports, 558, 1

Xu K., Jing Y. P., Zhao G.-B., Cuesta A. J., 2023, Nature Astronomy, 7, 1259

Yuan S., Eisenstein D. J., Garrison L. H., 2017, Monthly Notices of the Royal Astronomical Society, 472, 577

Yuan S., et al., 2024, Monthly Notices of the Royal Astronomical Society

Zhou R., et al., 2023, The Astronomical Journal, 165, 58

van Uitert E., Joachimi B., 2017, Monthly Notices of the Royal Astronomical Society, 468, 4502

Author Affiliations

[1]*Center for Astrophysics | Harvard & Smithsonian, 60 Garden Street, Cambridge, MA 02138, USA*
[2]*Departamento de Física, Universidad de los Andes, Cra. 1 No. 18A-10, Edificio Ip, CP 111711, Bogotá, Colombia*
[3]*Observatorio Astronómico, Universidad de los Andes, Cra. 1 No. 18A-10, Edificio H, CP 111711 Bogotá, Colombia*
[4]*Lawrence Berkeley National Laboratory, 1 Cyclotron Road, Berkeley, CA 94720, USA*
[5]*Physics Dept., Boston University, 590 Commonwealth Avenue, Boston, MA 02215, USA*
[6]*Dipartimento di Fisica "Aldo Pontremoli", Università degli Studi di Milano, Via Celoria 16, I-20133 Milano, Italy*
[7]*Department of Physics & Astronomy, University College London, Gower Street, London, WC1E 6BT, UK*
[8]*Instituto de Física, Universidad Nacional Autónoma de México, Cd. de México C.P. 04510, México*
[9]*University of California, Berkeley, 110 Sproul Hall #5800 Berkeley, CA 94720, USA*
[10]*Institut de Física d'Altes Energies (IFAE), The Barcelona Institute of Science and Technology, Campus UAB, 08193 Bellaterra Barcelona, Spain*
[11]*Institut d'Estudis Espacials de Catalunya (IEEC), 08034 Barcelona, Spain*
[12]*Institute of Cosmology and Gravitation, University of Portsmouth, Dennis Sciama Building, Portsmouth, PO1 3FX, UK*
[13]*Institute of Space Sciences, ICE-CSIC, Campus UAB, Carrer de Can Magrans s/n, 08913 Bellaterra, Barcelona, Spain*
[14]*Fermi National Accelerator Laboratory, PO Box 500, Batavia, IL 60510, USA*
[15]*Center for Cosmology and AstroParticle Physics, The Ohio State University, 191 West Woodruff Avenue, Columbus, OH 43210, USA*
[16]*Department of Physics, The Ohio State University, 191 West Woodruff Avenue, Columbus, OH 43210, USA*
[17]*The Ohio State University, Columbus, 43210 OH, USA*
[18]*School of Mathematics and Physics, University of Queensland, 4072, Australia*
[19]*Sorbonne Université, CNRS/IN2P3, Laboratoire de Physique Nucléaire et de Hautes Energies (LPNHE), FR-75005 Paris, France*
[20]*NSF NOIRLab, 950 N. Cherry Ave., Tucson, AZ 85719, USA*
[21]*Institució Catalana de Recerca i Estudis Avançats, Passeig de Lluís Companys, 23, 08010 Barcelona, Spain*
[22]*Department of Physics and Astronomy, Siena College, 515 Loudon Road, Loudonville, NY 12211, USA*
[23]*Department of Physics & Astronomy and Pittsburgh Particle Physics, Astrophysics, and Cosmology Center (PITT PACC), University of Pittsburgh, 3941 O'Hara Street, Pittsburgh, PA 15260, USA*
[24]*Departamento de Física, Universidad de Guanajuato - DCI, C.P. 37150, Leon, Guanajuato, México*
[25]*Instituto Avanzado de Cosmología A. C., San Marcos 11 - Atenas 202. Magdalena Contreras, 10720. Ciudad de México, México*
[26]*Instituto de Astrofísica de Andalucía (CSIC), Glorieta de la Astronomía, s/n, E-18008 Granada, Spain*
[27]*Departament de Física, EEBE, Universitat Politècnica de Catalunya, c/Eduard Maristany 10, 08930 Barcelona, Spain*
[28]*Department of Astronomy, The Ohio State University, 4055 McPherson Laboratory, 140 W 18th Avenue, Columbus, OH 43210, USA*
[29]*Department of Physics and Astronomy, Sejong University, Seoul, 143-747, Korea*
[30]*CIEMAT, Avenida Complutense 40, E-28040 Madrid, Spain*
[31]*Department of Physics, University of Michigan, Ann Arbor, MI 48109, USA*
[32]*University of Michigan, Ann Arbor, MI 48109, USA*
[33]*National Astronomical Observatories, Chinese Academy of Sciences, A20 Datun Rd., Chaoyang District, Beijing, 100012, P.R. China*

Many people made this work possible – this is just a list of the universities they're from!

33 institutions,
10 different countries

APPENDIX A: MODELLING DERIVATION

This FINAL page has some bonus math. I saved it just for you.

To compute the expectation v... ...orrelation between projected shapes and the 3D matter field, $\mathcal{E}_{\rm model}$, we begin with their definitions, as described in Eq...

$$\epsilon = \tau[T_{xx} - T_{yy} + 2iT_{xy}] \quad \text{(A1)}$$

$$Q(R_{\rm bin}, \pm\Pi_{\rm max}) = \frac{\int d^3 r W(\bar{r}) \delta e^{2i\theta_r}}{\int d^3 r W(\bar{r})(1+\xi_{\epsilon g})} \quad \text{(A2)}$$

Using these, $\mathcal{E}_{\rm model}$ is computed as:

$$\mathcal{E}_{\rm model} = \Re\langle\epsilon * Q\rangle = \frac{1}{2}\langle\epsilon^* Q + \epsilon Q^*\rangle = \Re\epsilon\Re Q + \Im\epsilon\Im Q = |Q|[(\epsilon_{xx} - \epsilon_{yy})\cos 2\theta + 2\epsilon_{xy}\sin 2\theta]$$
$$= \frac{-\tau}{\int d^3 r W(\bar{r})(1+\xi_{\epsilon g})}\int dz \int RdR \int d\theta W(\bar{r})\delta(R,z)[(T_{xx} - T_{yy})\cos 2\theta + (2T_{xy} - T_{xx} - T_{yy})\sin 2\theta] \quad \text{(A3)}$$

The 3 dimensions we integrate over here are the projected angle on the plane of the sky θ, the projected distance, R, and the redshift z. $*$ indicates complex conjugation and x^* is the complex conjugate of x. To compute the second integral, we convert to Fourier space.

$$\int dz \int RdRW(\bar{r}) \int d\theta \int \frac{d^3k}{(2\pi)^3}\tilde{\delta}(k)e^{-ik\cdot r}\int \frac{d^3q}{(2\pi)^3}e^{iq\cdot(0)}\tilde{\delta}q\frac{1}{q^2}[(q_x q_x - q_y q_y)\cos 2\theta + (2q_x q_y - q_x q_x - q_y q_y + \frac{2}{3}q^2)\sin 2\theta]$$
$$= \int dz \int RdRW(\bar{r}) \int \frac{dk_z}{2\pi}\int \frac{KdK}{(2\pi)^2}P(k)\int d\phi \int d\theta e^{-iK\cdot R - ik_z z}\frac{1}{k^2}$$
$$[K^2(\cos^2\phi - \sin^2\phi) \ldots (2\cos\phi\sin\phi - (\cos^2\phi + sin^2\phi))\sin 2\theta + \frac{2}{3}k^2\sin 2\theta] \quad \text{(A4)}$$

$\tilde{\delta}$ is the fractional overdensity in Fourier space. k represented the ... Fourier space, K represents the 2D position on the plane of the sky (k_x, k_y), and k_z along the line of sight. $k^2 = K^2 + k_z^2$. We the... ...ane wave expansion $e^{iK\cdot R} = \sum_{n=-\infty}^{\infty} i^n J_n(KR)e^{in\psi}$, where $\cos\psi = \hat{K}\cdot\hat{R}$. The above expression will integrate to 0 for all n except $n = \pm 2$, allowing us to reduce $e^{iK\cdot R}$ to $-2J_2(KR)e^{2i(\theta-\phi)}$, of which the real component is $-2J_2(KR)\cos(2(\phi-\theta))$. The inner integrands becomes:

To learn more about DESI, check out desi.lbl.gov

$$-\int_0^{2\pi} d\phi \int_0^{2\pi} d\theta 2J_2(KR)\cos 2(\phi-\theta)\left[K^2\cos 2\ldots K^2 \ldots \frac{2}{\ldots}(K^2 + k_z^2)\sin 2\theta\right] = -4\pi^2 J_2(KR)K^2 \quad \text{(A5)}$$

This leads to our final expression,

$$\mathcal{E}_{\rm model} = \frac{-\tau}{\int d^3 r W(\bar{r}\ldots}\int d^3 r W(\bar{r})\int \frac{dk_z}{2\pi}\int KdKJ_2(KR)\frac{K^2}{k^2}P_{gm}(k)e^{ik_z z} \quad \text{(A6)}$$

This is solved nu... ...erically, except for

$$\mathcal{J}_2(K) = \frac{2}{(R_{\rm max}^2 - R_{\rm min}^2)}\int_{R_{\rm min}}^{R_{\rm max}} \ldots \quad \text{(A7)}$$

for which we use the analytic solution:

This is the fourth paper summary like this I've made.
For one on the discovery of dark energy, see this link.
For ones on how galaxy alignment messes up measurements of the universe, see this link and also this link.

$$\mathcal{J}_2(K,R) = \frac{2}{(R_{\rm max}^2 - R_{\rm min}^2)}\frac{1}{K^2}[2J_0(KR_{\rm min}) + KR_{\rm min}J_1(KR_{\rm min}) - 2J_0(KR_{\rm max}) - KR_{\rm max}J_1(KR_{\rm max})] \quad \text{(A8)}$$

This paper has been typeset from a TeX/LaTeX file prepared by the author.

If you've gotten this far, CONGRATULATIONS!
I hope my notes made it easier to digest this paper. If you're a scientist, I would love to read similar notes on one of your papers :)
– Claire Lamman

I made this in power point using the XKCD font:
https://github.com/ipython/xkcd-font